

THERMAL REMOTE MONITORING OF NORRIS GEYSER BASIN AND
ASSOCIATED GEOTHERMAL RESOURCES, YELLOWSTONE NATIONAL PARK

FINAL REPORT

May 05, 2009

National Park Service CESU
Thermal Remote Monitoring of the Norris Geyser Basin, Yellowstone National Park
Agreement No. H1200040001, Task Agreement No. J1580050583, Task Order No.
UMT-26.

UM Application No. M2006-024
Carl Seielstad and LLoyd Queen, Forestry

2009 End-of-Grant Report

This effort has been funded through a Cooperative Ecological Study Unit (CESU) agreement between Yellowstone National Park's Geology program and The University of Montana- Missoula Department of Forest Management.

Disclaimer: The views expressed are the authors and do not necessarily represent the views of Yellowstone National Park, the Department of Interior or the United States Government.

Executive Summary

The Yellowstone Geothermal Monitoring Working Group was formed in 2005 to develop and evaluate monitoring methods and protocols and to provide baseline data for key geothermal systems within Yellowstone National Park (YNP). Cooperators included scientists from YNP, Montana State University, The University of Montana, and Utah State University. This report documents The University of Montana's contributions to thermal remote monitoring of Yellowstone National Park's geothermal features. The University of Montana received \$40,000 through the National Park Service Cooperative Ecosystem Studies Unit (CESU) in 2005 to acquire, process, and analyze fine-grained thermal remote sensing data from the Norris Geyser Basin and surrounding areas. In 2006, The University of Montana received an additional \$40,000 to reacquire data within the Mammoth-Norris corridor and at other locations in and adjacent to the YNP.

This report describes the acquisition parameters, data, and processing methods, it provides a preliminary assessment of radiant flux in the Norris Geyser Basin, and it presents lessons learned and recommendations for Geothermal Monitoring in Yellowstone National Park. It is accompanied by a hard drive containing raw and processed thermal data, ancillary field and GIS data, and documentation, serving as a primary source of metadata for that drive.

The work described herein is largely based on Hardy (2005), who acquired the first airborne thermal infrared images of Norris Geyser Basin in 2002. Hardy obtained two sets of imagery, one at midday and the other at night, with the goals of producing a suite of thermal attributes useful for indentifying, classifying and mapping geothermal features. His study forms a methodological basis for subsequent work, provides a baseline for comparative purposes, and identifies shortcomings that we have attempted to address in the 2005 and 2006 acquisitions. His work is referenced heavily in this report, but readers are referred to the source (Hardy, 2005) for technical and methodological details of the 2002 acquisitions.

Thermal infrared remote sensing data of the Norris Geyser Basin and the Mammoth-Norris corridor were obtained on October 09, 2002 using Airborne Data System's SpectraView sensor system (Hardy, 2005). On October 06, 2005, ADS SpectraView was utilized again to reacquire thermal data from Norris Geyser Basin. On October 11-12, 2006, the US Forest Service PSW FireMapper sensor package was used to obtain thermal imagery from Norris Geyser Basin, Mammoth, and Mud Volcano areas. The latter two acquisitions form the basis for this report. As noted previously, this report is

accompanied by associated image and vector data, which are provided on an external hard drive.

1. Project Introduction and Goals

The Yellowstone volcanic system is changing rapidly in response to variations in movements of molten basalt beneath the caldera (Wicks et al., 2005), resulting in concurrent changes in the behavior of geothermal geyser basins at the surface. Observed changes in geothermal activity have provided impetus for development of a geothermal monitoring plan, which was initiated in 2005 through partial funding from the U.S. Congress. Remote sensing of hydrothermal features is an important part of the monitoring plan and is being used to document spatio-temporal characteristics of radiative heat flux within and between geyser basins and to enhance Yellowstone's geothermal inventory.

The National Center for Landscape Fire Analysis at The University of Montana has been working with the National Park Service to map and monitor hydrothermal features in Yellowstone since 2005 with the goals of (a) establishing baseline thermal conditions; and (b) testing multiple instruments and sampling procedures in order to develop standard operating protocols for long-term monitoring. Their work is based on the exploratory efforts of Hardy (2005), who acquired and analyzed thermal imagery from Norris Geyser Basin in 2002. Hardy (2005) developed methods for identifying, classifying, and mapping thermal features using a single channel thermal sensor mounted aboard a fixed-wing aircraft. His work represents the initiation of fine-grained remote thermal monitoring of geyser basins in YNP and provides foundation for additional research into multi-sensor/platform characterization of geothermal features. Briefly, Hardy (2005) utilized day/night thermal infrared imagery from the 3-5 μm region of the electromagnetic spectrum to develop a suite of thermal attributes, including radiant temperatures, day-night temperature differences, and apparent thermal inertia (the latter attribute requiring albedo estimates derived from complementary imagery in the visible-NIR portion of the EMR (~0.45-0.95 μm)). Dynamic thermal calibration was used to exploit natural, pseudo-invariant reference targets instrumented with *in situ* kinetic temperature recorders.

In late 2005, a second set of thermal images was acquired for the Norris Geyser Basin using the same system as Hardy (2005), in an effort to further substantiate baseline thermal conditions within the Basin and to document changes. The major difference between the two acquisitions is that the data from the second mission was processed in-house in order to retain the 12-bit characteristics of the raw data and to address the image striping that was observed in data from the first mission. The primary outcomes from the 2005 acquisition are an assessment of sub-Basin spatial variations in geothermal flux and a basin-wide flux comparison between 2002 and 2005.

In October of 2006, an additional acquisition of thermal data was obtained, this time using a calibrated 8-14 μm imaging system. The intent of this most recent acquisition

was five-fold: first, to provide comparative data for a known geothermal landscape (Norris Geyser Basin) from a different imaging system; second, to test the feasibility of collecting data from multiple dispersed targets within a single mission; third, to demonstrate the ability to produce quick-look imagery for rapid assessment of hydrothermal features; fourth, to compare and contrast the strengths and weaknesses of a multi-channel imaging system with the system that was used in 2005; and fifth, to acquire thermal data within a vapor dominated geothermal system. To meet the stated intent, data were acquired for Norris Geyser Basin, Mud Volcano, Mammoth Terrace, and LaDuke Hotsprings.

2. Image Acquisition

2.1. 2002 Acquisition (Hardy, 2005)

Description: Norris Geyser Basin northward, including Roaring Mountain. Northwest-Southeast Flightlines with 60% endlap and 30% sidelap. Two acquisitions (day and night). Mean flying height: 1200 m AGL. Flight speed: 190 knots.

Date: October 09, 2002.

Time: Day (1210 – 1450 MDT); Night (1850-2030 MDT)

Weather: wind SW 12-16 gust to 21 kph. Min/Max temp 6.7/-2.8C. Min/Max RH 68/47%.

Antecedent Weather: Dry on day of acquisition and previous two. Light rain (0.007in) three days prior to acquisition.

Instrument: Airborne Data Systems SpectraView (Redwood Falls, MN), with Kearfott 4920 IMU (ring gyro) and integrated differential GPS, flown aboard a Piper Seneca. Aircraft guidance software used with automated shutter control. SpectraView system includes a 5-channel sensor package (more info below).

2.2. 2005 Acquisition

Description: Norris Geyser Basin northward, including Roaring Mountain. North-South Flightlines with 60% endlap and 30% sidelap. Two acquisitions (day and night). Mean flying height: 1220 m AGL. Flight speed: 190 knots.

Date: October 06, 2005.

Time: Day (1230 – 1530 MDT); Night (1830-1930 & 2115 – 2315 MDT- sensor malfunction required shutdown from 1930 – 2115 MDT).

Weather: West winds 13-40 kph during day acquisition. Air temperature in Norris Geyser Basin: 6.5 – 7.0 C. Minimum RH during day was 76%. During night acquisition, winds downslope/down valley at 5-8 kph. Air temperature in Norris Geyser Basin: 0.8 – -0.8 C. Maximum RH during night was 89%.

Antecedent Weather: 10-15 cm of wet snow the night before acquisition, with light rain on the three previous days. Min/Max temps on previous day were 0.55/-6.7C. Min/Max RH was 96/81%.

Instrument: Airborne Data Systems SpectraView (Redwood Falls, MN), with Kearfott 4920 IMU (ring gyro) and integrated differential GPS, flown aboard a Piper Seneca.

Aircraft guidance software used with automated shutter control. SpectraView system includes a 5-channel sensor package.

2.3. 2006 Acquisition

Description: Multiple acquisitions on Oct 11 and 12, 2006 with ~10% endlap and ~25% sidelap. Mean flying heights: 3500 – 4000 meters MSL translating to 1200-1600 meters AGL. Flight speed: 185 knots.

Norris Geyser Basin (Oct. 11, 2006, 1811 – 1850 MDT (night))
Mud Volcano Area (Oct. 11, 2006, 1902 – 1920 MDT (night))
Mammoth Hot Springs (Oct. 11, 2006, 1930 – 1949 MDT (night))
Old Faithful Area (Oct. 11, 2006, 1750 – 1800 MDT (night))

Norris Geyser Basin (Oct. 12, 2006, 1419 – 1455 MDT (day))
Mud Volcano Area (Oct. 12, 2006, 1354 – 1408 MDT (day))
Mammoth Hot Springs (Oct. 12, 2006, 1503 – 1529 MDT (day))
Yellowstone River to La Duke (Oct. 12, 2006, 1538 – 1550 MDT (day))
Old Faithful/Firehole Area (Oct. 12, 2006, 1602 – 1612 MDT (day))

Norris Geyser Basin (Oct. 12, 2006, 2004 – 2048 MDT (night))
Mud Volcano Area (Oct. 12, 2006, 2104 – 2117 MDT (night))
Mammoth Hot Springs (Oct. 12, 2006, 1858 – 1910 MDT (night))
Yellowstone River to La Duke (Oct. 12, 2006, 1914 – 1935 MDT (night))

Dates: October 11-12, 2006.

Time: see above.

Weather: wind W-NW 6-10 gust to 12mph. Min/Max temp was 10/-1.1C. Min/Max RH was 78/45%.

Antecedent Weather: Similar weather to acquisition days on previous two days. Light rain (0.015in) 3 days previous. Min/Max temps on previous day were 8.3/0.56F. Min/Max RH was 85/46%.

Instrument: FireMapper (US Forest Service Pacific Southwest Research Station, Riggan and Hoffman, 2003), with integrated differential GPS/INS, flown aboard a Piper Navajo.

3. Sensor Descriptions

3.1. Airborne Data Systems SpectraView (used in 2002 and 2005)

3.1.1. Camera Parameters:

Pulnix TM-1001 Visible/NIR cameras fitted with 12.5 mm focal-length lens. CCD arrays of 999 x 1016 pixels at 9 microns per pixel. Nominal 0.88 m ground resolution cell at specified flying height (879 x 894 m scene).

Cincinnati IRRIS-256ST MIR camera fitted with 13 mm focal-length lens. CCD array of 256 x 256 pixels at 30 microns per pixel. Nominal 2.8 m ground resolution cell at specified flying height (717 x 717 m scene). Camera has band passes at 3.6-4.1 and 4.5-5.1 microns, 12-bit radiometric resolution, 256x256 pixel InSb focal plane array. It is cooled with a small sterling cycle cooler. Output is raw digitized signal. The camera has four temperature ranges that set max/min observable temperature as well as sensitivity. Both 2005 data sets were acquired in Range 2. (Note that the 2002 acquisitions by Hardy (2005) were obtained in Range 1.

IRRIS-256ST Temperature Measurement (degrees C)

Range	Minimum	Maximum
1	-40	45
2	-20	80
3	40	150
4	100	300

ADS SpectraView Band Passes

Blue (8bit)	0.46-0.52 μm	Pulnix TM-1001 (with 12.5mm lens)
Green (8bit)	0.54-0.60 μm	Pulnix TM-1001 (with 12.5mm lens)
Red (8bit)	0.64-0.70 μm	Pulnix TM-1001 (with 12.5mm lens)
NIR (8bit)	0.77-0.97 μm	Pulnix TM-1001 (with 12.5mm lens)
TIR (12bit)	3.6-4.1 & 4.1-5.1 μm	Cincinnati IRRIS-256ST (with 30mm lens)

3.2. USFS- PNW Firemapper (used in 2006)

3.2.1. Camera Parameters:

FireMapper is part of a multi-camera system, which includes two Kodak MegaPlus 1.6i cameras equipped with 20mm lenses (1528 x 1024 array, IFOV = 0.45 mrad) and a SU320 digital camera with a 320 x 240 pixel InGaAs focal plane array operated at 1.58 μm (25mm lens, IFOV = 1.6 mrad). The FireMapper itself refers to the TIR instrument.

FireMapper (327 x 205 array, IFOV = 1.85 mrad) incorporates an uncooled, microbolometer focal-plane array in a multiple-channel imager (manufactured by Lockheed Martin IR Imaging Systems, 1999). Channels are implemented with a filter

wheel which provides two narrow bands, with wavelengths of 8.1 to 9 micron and 11.4 to 12.4 micron, and a broad band encompassing the entire range from 8.1 to 12.4 micron. Atmospheric corrections of FireMapper data are made using local water vapor measurements and the Modtran atmospheric transmission model.

FireMapper Band Passes

Red (10bit)	0.615-0.685 μm	Kodak MegaPlus 1.6i (with 20mm lens)
NIR (10bit)	0.815-0.885 μm	Kodak MegaPlus 1.6i (with 20mm lens)
MIR (10bit)	1.50-1.65 μm	Sensors Unlimited, Inc. InGaAs Model SU320M (with 25mm lens)
TIR (16 bits)	8.1 – 9.1; 11.4 – 12.4; 8.1 – 12.4 μm	FireMapper (Space Instruments, Inc.) (with 25mm lens)

The FireMapper has two levels of onboard offset calibration that are used during flight. The FireMapper performs a through-the-lens absolute offset calibration upon user command. This calibration uses an ambient-temperature reference blackbody with very high emissivity and known temperature that is mounted below the lens. A reference blackbody calibration, which is typically accomplished prior to the start of a remote-sensing flight line, also serves to remove image patterns caused by thermal emissions within the instrument and reflections from the band-pass filters that would otherwise seriously confound the target imagery. A second level of offset calibration, for control of drift in the microbolometer, is automatically provided by imaging a small blackbody mounted in the FireMapper filter wheel.

Radiance calibrations for each of the FireMapper channels have been performed in the laboratory with a high-precision, high-temperature blackbody radiation source that has been calibrated with reference to six primary-standard freeze-point blackbodies. The radiance calibration of each channel is highly linear on the instrument digital number.

Ground cell resolutions: Kodak Cameras: Nominal 0.32 m ground resolution cell at 1400 m flying height (499 m x 328 m scene). Sensors Unlimited Camera: Nominal 1.14 m ground resolution at 1400 m flying height (366 m x 274 m scene). FireMapper: Nominal 1.32 m ground resolution at 1400 m flying height (432 m x 271 m scene).

4. Image Processing

4.1. 2005

4.1.1. Introduction

ADS data are delivered in binary format (.raw) and as ortho-rectified scenes (.tif). The ortho-rectification is performed by ADS using proprietary automated routines that perform band-to-band registrations and that incorporate standard rotations developed from unprocessed GPS and INS roll, pitch, and yaw data. ADS does not bore site their cameras and in our experience, their ortho-rectifications are adequate for surveillance purposes when images are acquired under ideal atmospheric conditions, and inadequate for most reasonable purposes when the atmosphere is turbulent. This is not atypical of other instrumentation that we have worked with in the domain of fire mapping. For the 2005 Norris Geyser Basin acquisitions, the automated ortho-rectification was less than ideal, resulting in our decision to re-process the data manually using image blocks and tie-points. Good results can be obtained by the latter method, which is costly and extremely time consuming.

4.1.2. Data Format and Import

Raw data from the ADS Spectraview system are stored as band-sequential 8-bit series in the order blue, green, red, NIR, TIR. Each file is represented by 4,192,256 bytes, where the blue, green, red, and NIR channels are $x = 999$ and $y = 1016$ (8 bits per cell). The TIR is digitized as 12-bit data, but stored as 16-bit data where $x = 256$ and $y = 256$ (16-bits per cell).

Each of the visible and NIR bands contains 26,464 header and 26,464 trailer bytes (total number of bytes for Ch1 – Ch4 is 4,061,184, leaving 131,072 bytes for the MIR (Ch5). To import one of the visible-NIR channels and generic binary, one must sum the antecedent header, trailer and band bytes (e.g., 26,464 bytes per header or trailer and 1,014,984 per band) to define the appropriate number of header bytes, use 1016 rows x 999 columns, swapped bytes (Motorola Chipset), and unsigned 8-bit format. To import the TIR data as generic binary, one must use 4,061,184 header bytes, 256 rows x 256 columns, swapped bytes (Motorola Chipset), and unsigned 16-bit format.

4.1.3. Destriping

The ADS Spectraview TIR data are characterized by a distinct vertical striping (bias), in which every other column is consistently brighter than its neighbors. This phenomena was noted in 2002 by Hardy (2005) and is again apparent in our 2005 data. The SpectraView TIR system uses two sets of amplifiers to perform the analog-to-digital conversion (Hardy, 2005). Consequently, if the electronics are not cross-calibrated, adjacent columns of data will not be equivalent. Unfortunately, once the data are geo-processed, the striping bias becomes difficult to remove because it no longer consistently occurs in columns but rather is woven into the scenes. Hardy (2005) addressed the issue through filtering because he was working with vendor-provided ortho-rectified scenes. We chose to address the striping issue in the raw data and perform the ortho-corrections ourselves.

Our destriping approach was as follows. 1) Identify large, homogenous cold and hot features in the images; 2) Difference adjacent columns in these areas on the assumption

that adjacent columns are sampling the identical temperature regimes; 3) evaluate mean and standard deviation differences between adjacent columns to quantify striping (e.g., within column standard deviations should be ~equal for adjacent columns while means should be systematically offset); 4) apply striping offset to up-weight striped columns.

We used warm sinter backgrounds in Norris Geyser Basin (scene068) as hot targets (410-440 DNs) and large water bodies (scene0774) as cold targets (261 – 279 DNs). Within column standard deviations were insignificantly different from column to column while means differed by 15.33 to 15.97. Overall mean differences between paired ‘like’ columns (every other column) was 0.095 while mean difference between adjacent columns was 15.87. Consequently, we chose to up-weight every other column by 16 DNs, resulting in visibly destriped images that exhibited no column-to-column bias (as determined by t-tests on 100 random column pairs).

4.1.4. Band-to-Band Registration

The five individual cameras in the ADS SpectraView system are not bore-sited, thus requiring band-to-band registration (e.g., each band within a scene is not exactly coincident with its companion bands). However, with very few exceptions, the lack of coincidence between bands was the same for each scene, allowing a single solution for each band to be applied to all scenes. We used scenes from the Mammoth, WY town site to perform the band-to-band registration because they offered the most distinct and easily identified ground control points in the study area.

Each band was registered to SpectraView Band3 (Red) by identifying distinct tie points common to the respective image pairs. Collections of tie points were iteratively added and evaluated in terms of relative contribution to model error. A second order polynomial was used to transform the coordinates of each band to match the geometry of band3. The cell size of the TIR band was reduced to match the resolution of the visible and NIR bands (e.g., the TIR image was resampled, effectively splitting each cell in the TIR image into roughly nine individual cells). The noted resampling was required in order to stack the images for ortho-rectification. RMSE of the four models ranged from 0.14 to 0.94 pixels.

4.1.5. Ortho-rectification

Ortho-rectification was performed on collections of individual image stacks in Leica Photogrammetry Suite (LPS) using Block Triangulation. Output was individual scene layer stacks at 1-meter resolution. The overall geometric accuracy of the daytime ortho-rectified imagery is 1.8 meters (RMSE). The source data for the orthorectification was a USGS 10-meter Digital Elevation Model and USGS 1-meter Color-Infrared Digital Ortho Quarter Quad air photos (DOQQs) acquired in 2000. Both data sets were obtained from the Wyoming Geographic Information Advisory Council (WGIAC) data access portal (<http://wgiac.state.wy.us>). It is worth reiterating that RMSE represents an average number and thus, many places within the Norris Geyser Basin with much larger error are obvious to the naked eye.

Block triangulation is the process of establishing the relationships between groups of images (blocks), a camera, and the ground. It requires identification of Ground Control Points in the image block and in the reference image, as well as tie points common to adjacent images within the block. Establishing the geometry of the camera relative to the ground and relating the camera position to a conventional projected coordinate system provides the means to correct for image and relief displacement (e.g., to produce orthographically correct scenes).

Manual block triangulation is extremely time-consuming and tedious. It requires significant trial and error and constant reassessment of GCP and tie point quality. Our original intention was to use the aircraft attitude data from the inertial navigation system (INS) to georeference the images directly, and several attempts were made to derive precise external orientation parameters (omega, phi, kappa plus elevation and location) from the attitude information provide by the INS/GPS. However, due to several unknowns in the Sensor/INS system, direct georeferencing was not possible. In theory, direct georeferencing is possible if the precise geometry between the cameras and GPS is known, and the GPS and INS data are finely resolved temporally and accurately corrected. However, in our experience, high quality direct georeferencing remains elusive to all but the most accomplished photogrammetric engineering solutions.

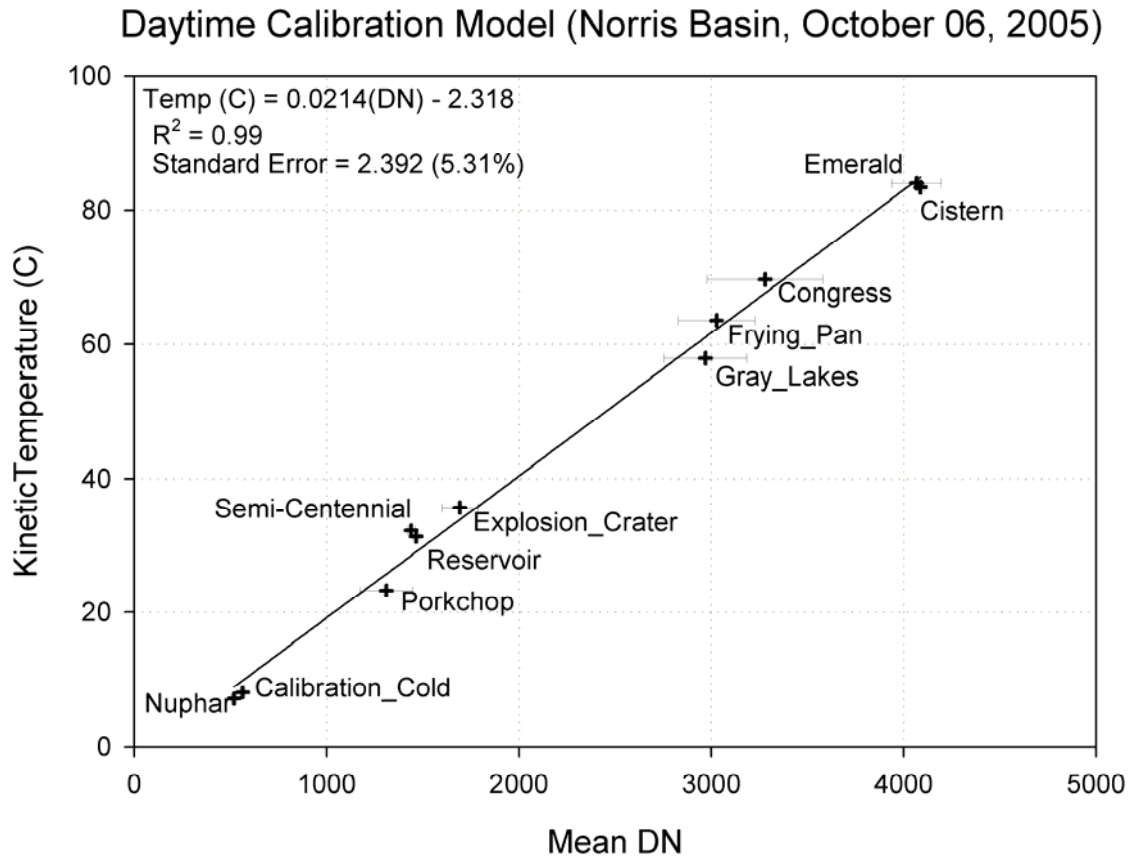
4.1.6. Mosaicking Images

Individual ortho-rectified image stacks were mosaicked using the MosaicPro module in Erdas Imagine 9.1. The TIR data were separated from the stack and mosaicked independently. Weighted seamlines were generated to force edges between images in the mosaic to follow homogeneous features and borders such as roads and rivers. Settings for the seam line refining parameters were as follows: Segment Length (in pixels) = 10; Bounding Width (in pixels) = 200; Pixel Value Similarity = 2; Direction = 0; Standard Deviation = 2.

4.1.7. Kinetic Temperature Calibration

We converted image digital numbers to kinetic temperatures by generating a model relating DN's to temperature data obtained from in situ temperature loggers. Prior to the acquisition, we installed HOBO kinetic temperature loggers in the surface boundary layer of eleven geothermal features in and around Norris Geyser Basin. They spanned a temperature range of 5 – 90 degrees Celsius. Within the image data, we extracted 1 – 9 connected cells (depending on the size of the thermal feature) at each logger location and calculate the average DN. Briefly, the target sample size was nine pixels, but several of the calibration features did not contain nine pixels. From the logger data, we averaged temperatures at plus/minus ten minutes of overpass. Finally, we compared the two via linear regression (figure below). It is worth noting that we extract DN's from the raw imagery, prior to any processing and consequently, match the locations of the loggers in the images contextually. The reason that we do this is because the resampling that

inevitably occurs during processing modifies, and in some cases removes key DNs from the relatively small geothermal targets in which the loggers are installed.



Assumptions of the calibration are the same as those adopted by Hardy (2005). They are:

1. The atmosphere is clear and dry.
2. Reflectance and emittance are Lambertian
3. Targets assume emissive properties of gray-bodies (emissivity not wavelength dependent).
4. Thermal loggers represent true kinetic temperatures of reference sites.
5. Kinetic temperatures of references are uniform for corresponding IFOV of sensor.
6. The relationship between DN's and at-sensor radiance is linear.

4.1.8. Emissivity Correction

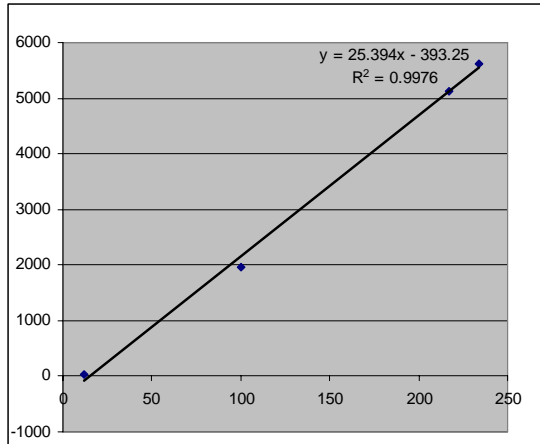
In order to produce radiant temperatures, we converted kinetic temperatures to Kelvins and used the equation:

$$Radiant\ Temp = Emissivity^{1/4} * Kinetic\ temp$$

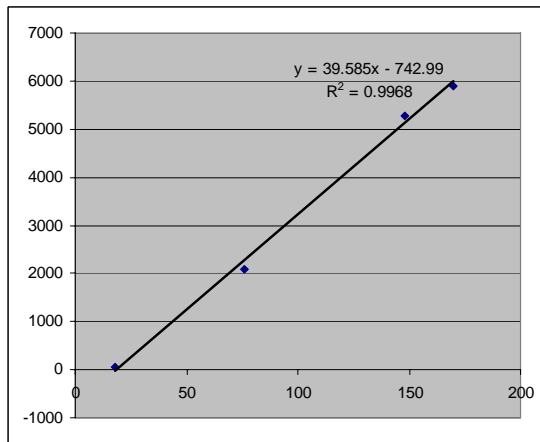
As with Hardy (2005), we applied one-minus-albedo as a proxy for emissivity. One-minus-albedo was derived from calibrated reflectance data in the green and NIR channels after Brest et al. 1987. Hardy (2005) validated this approach using the ADS data

acquired in 2002. To obtain calibrated reflectance, we regressed DNs from our imagery in the green, red and NIR bands against NASA AVIRIS RTCG DN's (same source as Hardy 2005) for a variety of targets in Norris Basin. Reflectance was obtained by scaling the RTCG DNs between 0 and 20,000.

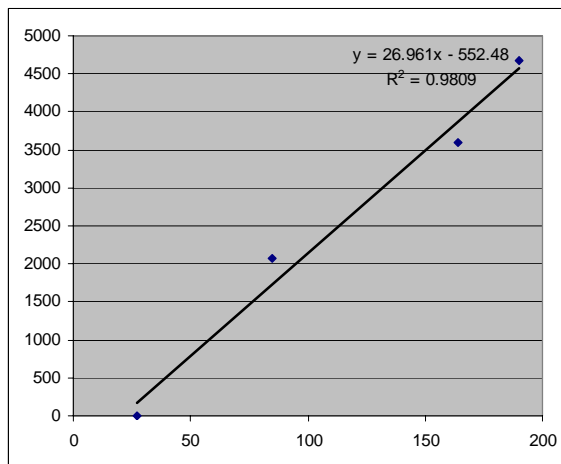
GREEN



RED



NIR



The crosswalk between AVIRIS RTCG bands and ADS bands is as follows:

ADS GREEN = RTCG 22 (layer 5)

ADS RED = RTCG 32 (layer 13)

ADS NIR = RTCG 56 (layer 27)

The target areas used for the calibration are: shaded water in Nuphar Lake, asphalt in Norris Basin parking lot, two moderately bright areas in the basin proper. It is worth noting that many areas in the Basin do not fit the reported calibration curves, perhaps because of substantial differences in surface moisture and illumination conditions.

A problem with the calibration of the ADS data is that the ADS bands saturate at relatively low reflectance.

Green saturates at: 0.3028413

NIR saturates at: 0.3020807

Therefore, all reflectance values greater than 0.30 are unknown, and all 1-albedo values less than 0.70 unknown. Candidate pixels are either snow or bare, light-colored ground. Snow should have an emissivity of 0.99 while the bare ground will have a much lower value. The distinction is important because bare ground areas may well be geothermal areas. One possible way to fix this problem is to use temperature to screen bare ground from snow. In the daytime imagery, temps of snow near 5C while temps of bare ground above 10C. However, even with correct classification, we still do not have a good method of populating bare ground pixels with emissivity.

1-albedo (~emissivity) is derived from calibrated ADS reflectance after Hardy (2005) after Brest and Goward (1987). In short, the landscape is classified as vegetation and non-vegetation by:

$\text{NIR/GREEN} > 2.0 = \text{vegetated.}$

$\text{NIR/GREEN} \leq 2.0 = \text{non-vegetated.}$

Then,

$\text{Vegetated Albedo} = 0.526(\text{GREEN}) + 0.362(\text{NIR}) + 0.112(0.5(\text{NIR}))$

$\text{Non-veg Albedo} = 0.526(\text{GREEN}) + 0.474(\text{NIR})$

1-albedo estimates for calibration targets are:

Nuphar Lake: 1.000

Semi-Centennial: 0.981

Reservoir: 0.955

Gray Lakes: 0.931

Emerald: 0.920

Explosion Crater: 0.900

Congress:	0.825	
Frying Pan:	0.825	
Cistern:	0.810	
Steamboat Channel:	0.760	
Cinder:	0.785	Cinder black cinders: 0.960

From an emissivity perspective, the 1-albedo values make qualitative sense, with one exception (Cistern). Water in Cinder is chalky white. Water in Frying Pan is chalky gray. Water in Congress is chalky blue. Water in Cistern is clear and perhaps should have an emissivity more like Emerald's (0.920).

4.1.9. Heat flux calculation

To quantify the heat energy from the thermal areas we calculated heat flux in watts per square meter via the Stefan-Boltzmann equation:

$$M = \sigma T^4$$

M = watts per meter²

σ = Stefan-Boltzmann constant 5.667×10^{-8}

T = radiant temperature in Kelvins

Legend

t_rad.img

Value

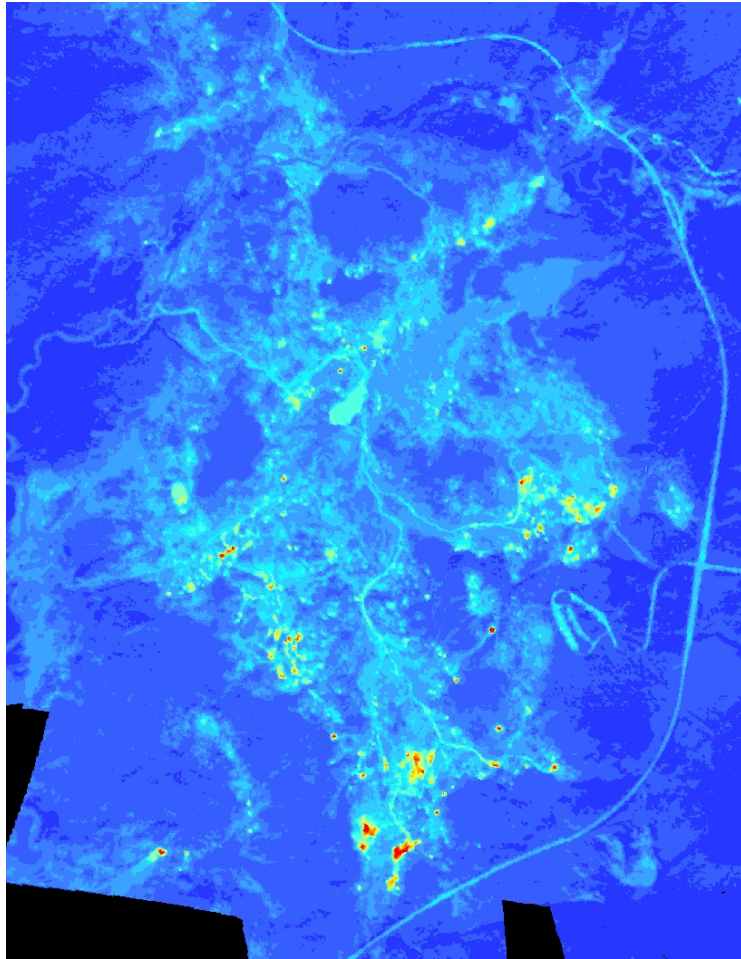
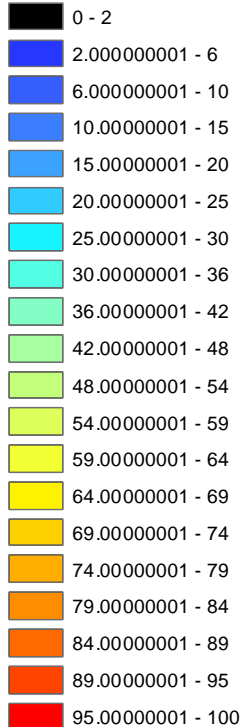


Figure 2. Radiant Temperature of Norris Geyser Basin, October 06, 2005, 1300-1500.

4.2. 2006

4.2.1. Introduction

The FireMapper System flown by the USFS PSW Research Station was used to acquire thermal data for several reasons. First, one of the primary purposes of our efforts was to evaluate different kinds of instruments. FireMapper represents an unusual example of a two-channel uncooled microbolometer system. Uncooled microbolometry potentially represents the future of high-quality, low cost thermal remote sensing because it does not require independent refrigeration. Second, the project required a proven ‘system’ with integrated GPS/INS, robust on-board calibration, and visible-NIR channels. Third, the instrument needed to be available on one day’s notice (due to thermal fog considerations in the YNP geyser basins), so needed to be located within a day’s flight of the study area. Additionally, the pilot and operator had to be able and willing to fly on such short notice. Fourth, the pilot and operator required experience flying targets on an ad-hoc, dynamic basis.

In practice, the former considerations proved advantageous and we managed to acquire data from multiple targets in a tight weather window. It is worth noting that the targets were flown at multiple elevations ranging from 1200-1600 meters AGL. Additionally, small data gaps occurred in Norris Geyser Basin and Mud Volcano.

The general approach to image processing of the 2006 data was the same as for the 2005 data; that is, calibration to in-situ kinetic temperature, ortho-rectification, conversion to radiant temperature, and radiant flux calculation. One notable difference is that the 2006 data were not adjusted for emissivity differences due to the absence of calibration data needed to calculate 1-albedo. All of the ortho-rectification was completed by PSW FireMapper staff and delivered as individual tiles.

4.2.2. Data Format and Import

FireMapper data are stored in binary format within .dat files that contain all images within an individual flightline. Image frames are extracted via a stand-alone utility called FireMapper Image Extraction Tools, a poorly documented but useful and necessary tool (in the case of this study, version 3.3.1.247). The extraction utility allows batch extraction of image bands, automated conversion to brightness temperature (degrees C) and several output options, including binary and comma separated text files. The utility also contains ephemeris for each frame, including timestamps, GPS-IMU data, and calibration information. Extracting to binary yields a .raw file for each image frame which can be imported into conventional image processing software using a generic binary format (for thermal channels: unsigned 16-bit data at 327 columns by 205 rows; for visible/NIR data: unsigned 10-bit at 1528 columns by 1024 rows; for mid-IR data: unsigned 10-bit at 320 columns by 240 rows).

4.2.3. Destriping

Not-Applicable.

4.2.4. Band-to-Band Registration

Band-to-band registration was conducted by PSW FireMapper Staff in ERDAS Orthobase Pro using auto-tie point generation.

4.2.5. Ortho-rectification

As described previously, ortho-rectification was completed by PSW FireMapper staff using the same process that was utilized in 2005. Day images were ortho-rectified in Leica LPS with manual tie points and GPS/IMU data. Night images were ortho-rectified only using GPS/IMU, resulting in a substantial reduction in geometric quality (a function of platform stability at time of acquisition). The native thermal images are 16-bit, calibrated to an internal blackbody within the sensor system. Resample was nearest neighbor. It is worth pointing out that the direct-georeferencing took much longer to complete than expected, resulting in a request for a no-cost extension. In short, the

FireMapper system is plagued with many of the same issues as the ADS system, requiring significant hands-on manipulation to produce data with consistent geometric properties. Additionally, even with the higher contrast imagery provided by the wide-band thermal channel (8-11microns), night scenes were not consistently geo-located to an acceptable standard. The latter issues were not anticipated and we conclude that the direct-georeferencing abilities of the PSW system have been greatly overstated. With that said, acceptable data can be obtained in ‘clean’ air without a lot of hands-on manipulation. FireMapper demonstrated this with the production of quick-look imagery from multiple, widely dispersed targets within a few days of acquisition.

It is also worth noting that FireMapper onboard-calibration results in clean imagery in the wideband thermal channel and this was the only thermal channel to be geo-rectified by the vendor. The two shortband-channels are much noisier and offset spatially due to the timelag of the filter wheel. Only raw data is available for the latter two channels.

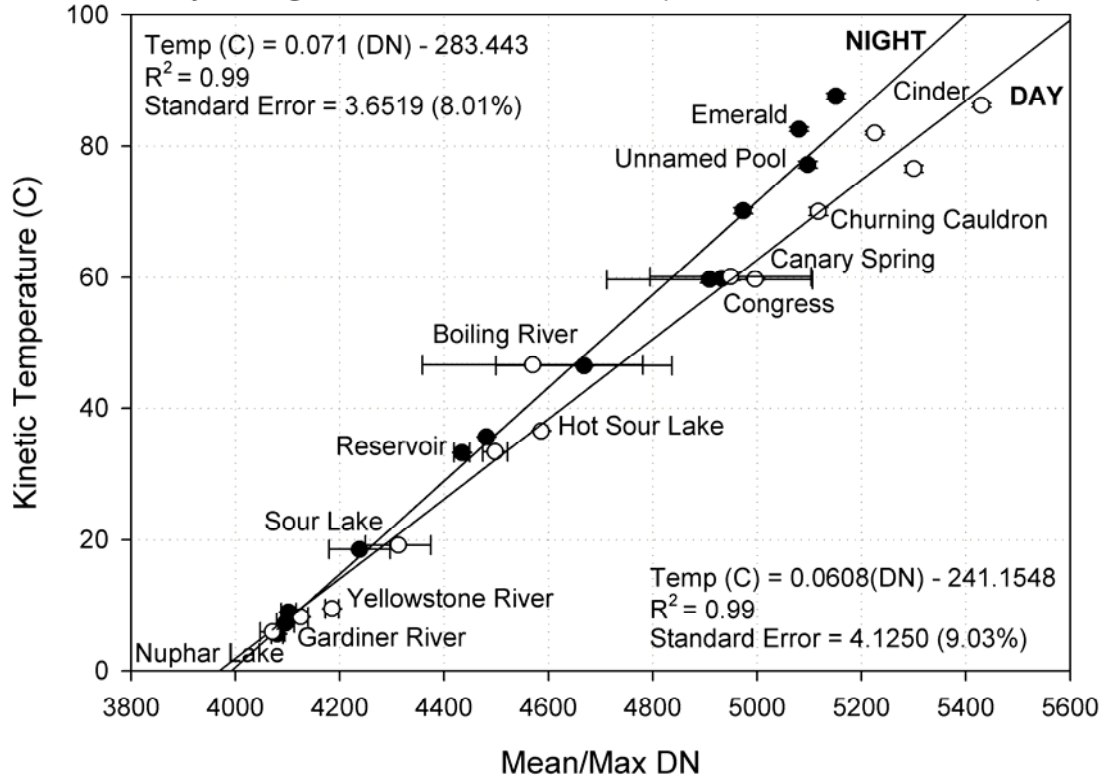
4.2.6. Mosaicking Images

Individual ortho-rectified image stacks were mosaicked using the MosaicPro module in Erdas Imagine 9.1. The TIR data were separated from the stack and mosaicked independently. Weighted seamlines were generated to force edges between images in the mosaic to follow homogeneous features and borders such as roads and rivers. Settings for the seam line refining parameters were as follows: Segment Length (in pixels) = 10; Bounding Width (in pixels) = 200; Pixel Value Similarity = 2; Direction = 0; Standard Deviation = 2.

4.2.7. Kinetic Temperature Calibration

We converted image digital numbers to kinetic temperatures by generating a model relating DN's to temperature data obtained from in situ temperature loggers. Prior to the acquisition, we installed HOBO kinetic temperature loggers in the surface boundary layer of twelve geothermal features in Norris Basin, Mammoth Hot Springs, and Mud Volcano geothermal area. They spanned a temperature range of 7 – 87 degrees Celsius. Within the image data, we extracted 1 – 9 connected cells (depending on the size of the thermal feature) at each logger location and calculate the average DN. For the small, more spatially discrete targets (Hot Sour Lake, Congress, Churning Cauldron, Unnamed Pool, Emerald, and Cinder), we used maximum DN instead of mean on the assumption that the pools were homogenous in temperature. From the logger data, we averaged temperatures at plus/minus ten minutes of overpass. Finally, we compared the two via linear regression (Figure below). The resulting model is used to convert DN's to kinetic temperatures. We extract DN's from the raw imagery, prior to any processing and consequently, match the locations of the loggers in the images contextually. The reason that we do this is because the resampling that inevitably occurs during processing modifies, and in some cases removes key DN's from the relatively small geothermal targets in which the loggers are installed.

Day & Night Calibration Models (YNP October 12, 2005)



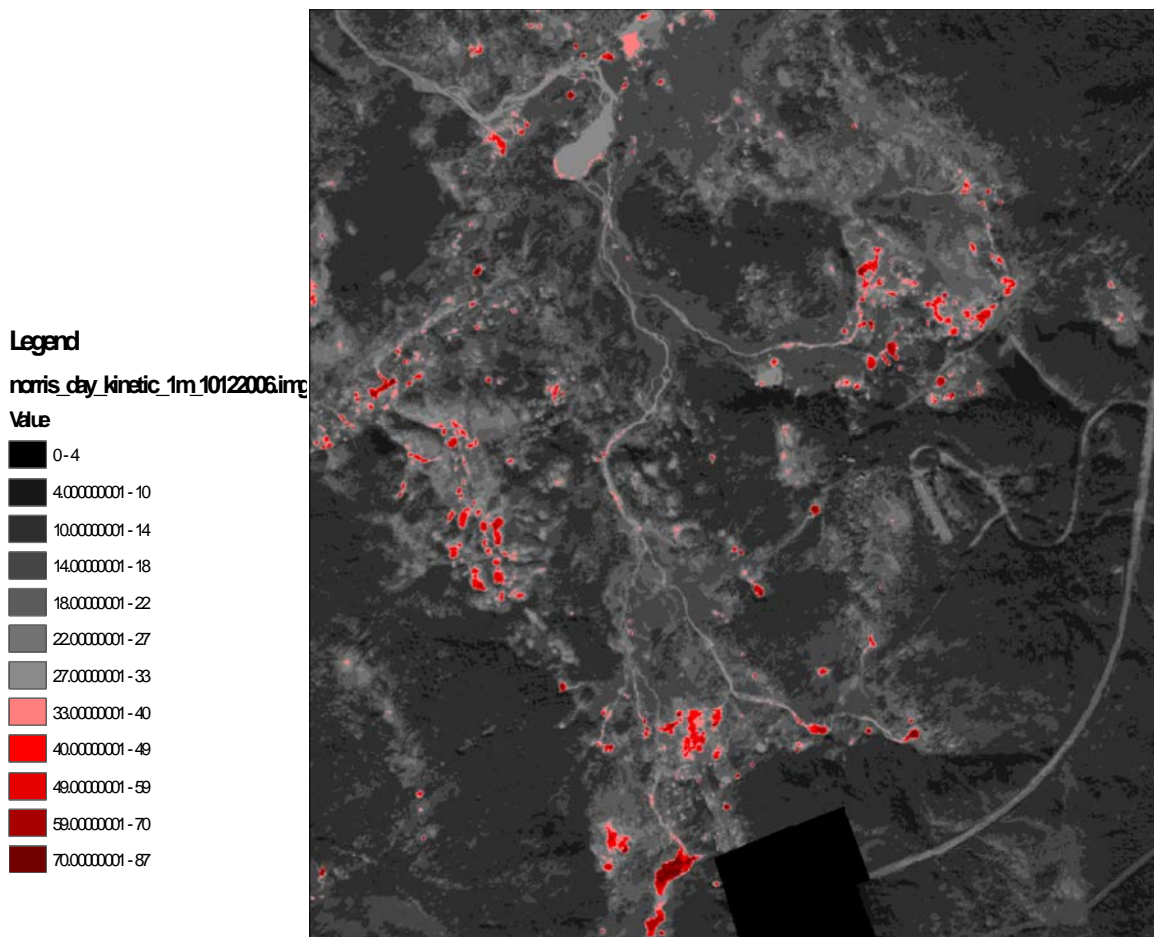


Figure 3. Kinetic temperature of Norris Geyser Basin, October 12, 2006, 1420-1455.

4.2.8. Emissivity Correction

As reported previously, the 2006 data were not adjusted for emissivity. In 2002 and 2005, 1-albedo was used as a proxy for emissivity (Hardy, 2005). One-minus-albedo was estimated from calibrated reflectance data in the green, red, and NIR channels after Brest et al. 1987. To obtain calibrated reflectance, DN's from 2002/2005 imagery in the green, red and NIR bands were regressed against NASA AVIRIS RTCG DN's (Hardy, 2005). This approach assumed that within-scene relative surface reflectance had not changed significantly since the NASA's AVIRIS data collection in 1999. A comparison of 2002 and 2005 emissivity layers suggests that this assumption was reasonable (with some previously mentioned exceptions within the sinter background of Norris Geyser Basin that were probably much wetter in 2005). It is possible that 1-albedo could still be derived from the red and NIR channels of FireMapper using a modified Brest et al. (1987) approach as described by Song et al. (1999), although this method will require additional scrutiny.

4.2.9. Heat Flux Calculation

To quantify the heat energy from the thermal areas we calculated heat flux in watts per square meter via the Stefan-Boltzmann equation:

$$M = \sigma T^4$$

M = watts per meter²

σ = Stefan-Boltzmann constant 5.667×10^{-8}

T = radiant temperature in Kelvins

5. Outcomes

5.1. Estimating Total Geothermal Energy Flux for Norris Geyser Basin, 2002-2006

The intent of this effort was to generate order-of-magnitude, basin-wide geothermal flux estimates for the Norris Geyser Basin. A primary issue was controlling for background flux under considerably different acquisition conditions on the three sampling dates. As described below, we stratified the Basin by dominant landcover types (forest, water, sinter, road) and sampled these landcovers for background flux outside of known geothermal areas. Our assumption is that the flux of landscapes adjacent to, but outside of known geothermal areas such as Norris Geyser Basin, is representative of background flux of within the basin. We use area weighted mean flux within each landcover class to produce total flux by a class. An exception was the sinter class, which does not often occur outside of geothermal areas. For the latter class, we use a minimum flux (5th percentile flux) on the assumption that this value represents flux without geothermal input.

5.1.1. Methods

5.1.1.1. Landcover Type Classification

1. 2002 visible bands were resampled up to 1.0-m² pixels (from 0.76 x 0.76-m)
2. 2002 and 2005 NDVI calculated
 - a. 2002: $(3 - 2) / (3 + 2)$; where 3 = NIR and 2 = red
 - b. 2005: $(4 - 3) / (4 + 3)$; where 4 = NIR and 3 = red
3. 2005 imagery recoded on the following ruleset:
 - a. Conditional statements assigned new category values according to the specified NDVI ranges:
 - NDVI ≤ -0.0703125 , 1 (water)
 - NDVI > -0.0703125 AND ≤ 0.0000 , 4 (snow)
 - NDVI > 0.000 AND < 0.25 , 3 (sinter)
 - NDVI ≥ 0.25 , 2 (forest)
4. Region grow tool was used to generate polygons from the recoded image
 - a. 4 neighbor-pixel option used, no islands allowed

- b. Generated AOI's were added to one of 3 new polygon shapefiles – water, forest, and snow
5. Shapefiles were edited to dissolve polygon boundaries, merge coincident polygons, fill holes, to snap polygons to adjacent polygons where appropriate, and to clip shapefiles to the Norris Geyser basin extent coincident with both the 2002 and 2005 data
6. The river was digitized and added to the water shapefile
7. Roads were digitized as a new shapefile
8. Using the ArcGIS erase tool, the 2005 sinter coverage was generated as the remaining basin area when the other 4 shapefiles were extracted (snow, water, forest, road) from the Norris Geyser Basin extent
9. 2002 imagery was then recoded
 - a. Conditional statements categorized NDVI pixels as either “water” or “not water”
 - $\text{NDVI} \leq -0.4375$, 2 (water), else 1 (not water)
10. Region grow tool and GIS processing as described above to generate a unique water coverage for 2002
11. Using the erase tool as for 2005, the 2005 forests, 2005 roads, 2005 snow, and 2002 water were extracted from the Norris boundary to generate the 2002 sinter coverage
 - a. 2005 snow is assumed to be grass/other in 2002
12. Individual shapefiles for 2002 and 2005 merged into one basin-wide shapefile for each year using the Union tool in Arc
13. Shapefiles converted to feature classes in a personal geodatabase to maintain updated area calculations

5.1.1.2. Flux Estimation

1. Using ArcGIS, polygon AOI shapefiles were created for representative landcover types for forest, water, road, snow, and grass
 - a. Goal was to select non-geothermal representative areas for each landcover type outside of the basin area
 - b. Google Earth imagery and NDVI grid used to select appropriate areas with similar landcover characteristics
2. Extract by mask function extracted the radiant flux grid cell values coincident with the AOI polygons
3. Cell statistics provided distribution information, and the mean value was selected as the representative background flux – this was repeated for each class except for sinter
4. It was assumed that the near-minimum flux value associated with sinter would be an appropriate estimate of the non-geothermal flux contribution for this landcover class. The 5th percentile value was selected to minimize the chance of selecting an erroneously low minimum value
5. Basinwide flux values were calculated for each landcover type by multiplying the total area in the landcover class (m^2) by the median flux value (W/m^2)

5.1.2. Discussion

In 2002, daytime total radiant flux for Norris Geyser Basin (not adjusted for background) was 1.22GW. In 2005, total unadjusted flux was 1.11GW. On the assumption that background flux was identical during both acquisitions (0.9GW (200w/m² * area of basin)), geothermal heat flux amounts to 0.32 GW in 2002 (day) and 0.21 GW in 2005 (day) for a difference of 0.11GW between the two years. In 2006, total daytime flux was 1.10GW, which given the assumption above, translates to 0.20 GW of geothermal flux.

The assumption of equal background flux is likely a poor one given observed differences in environmental conditions between acquisitions. Thus, it is logical to estimate background flux, as described above. Table L. below shows these results. In general, year-to-year flux as measured by the two instruments at different wavelengths across three years is consistent given potential confounding factors. Daytime background flux appears to represent about 88% (87.4 – 89.6%) of total flux, with the balance presumably attributable to geothermal flux. There is an ~11% difference in background flux between 2002 and 2005/2006 (larger flux in 2002), perhaps due to differences in moisture status of the ground surface. Given the uncertainties in background flux combined with noise from calibration and emissivity estimation, we conclude that there is no detectable change in flux from 2002 to 2006. Interestingly, if one partitions Norris Basin by radiant flux, very hot targets (>700W/m²) account for a fraction of a percent of total flux, e.g., heat from the ‘background’ sinter dominates total geothermal flux. From a synoptic thermal perspective, then, the geothermal features that culturally define Yellowstone geyser basins do not have the same status when it comes to contributing to system-wide flux.

Table L. Daytime Radiant Flux for Norris Geyser Basin (2002-2006)

BASINWIDE TOTALS	WATTS	GW	CHANGE FROM 2002
2002 TOTAL FLUX, DAY	1223413496.00	1.2234	
2002 GEOTHERMAL FLUX	135988140.00	0.1360	
2002 BACKGROUND FLUX	1081440551.00	1.0814	
			% CHANGE
2005 TOTAL FLUX, DAY	1110641929.00	1.1106	-10.15%
2005 GEOTHERMAL FLUX	136870192.80	0.1369	0.64%
2005 BACKGROUND FLUX	972028871.40	0.9720	-11.26%
			% CHANGE
2006 TOTAL FLUX, DAY	1095870000.00	1.0959	-11.64%
2006 GEOTHERMAL FLUX	113744094.58	0.1137	-19.56%
2006 BACKGROUND FLUX	982125905.42	0.9821	-10.11%

The night imagery acquired in each of the three years described in this study has been notoriously difficult to work with. Conventional wisdom suggests that imagery obtained at or near the peak of radiational cooling during a dry night should provide the cleanest representation of geothermal flux. In practice, two factors have complicated assessment of this notion. First, near surface water vapor (geothermal fog and boundary layer steam) appear to routinely obscure ground features even during ‘dry’ nights. The 2005 night imagery provides the most obvious example of this phenomenon. Geothermal features such as Cinder Pool, Green Dragon, and Congress Pool appear significantly colder than background, similar to the way cloud tops appear in MODIS and AVHRR thermal bandpasses. Second, the night imagery is difficult to geolocate, particularly in the shortwave thermal IR. Imagery in the shortwave thermal IR (3-5 μ m) is devoid of background context so the GPS/IMU solution needs to be nearly perfect to provide reasonable georeferencing (e.g., manual tie-point generation is not tractable). At longer wavelengths and lower radiometric resolution (8-14 μ m) background features are visible, but a relatively large IFOV combined with a low contrast background makes accurate tie-point generation difficult. The factors above resulted in night imagery with generally poor geometric fidelity and considerable measurement uncertainty.

Perhaps the best of the night imagery was obtained in 2006 with the FireMapper longwave thermal camera. Table N shows flux data for Norris Geyser Basin on October 11 (night), and October 12 (day and night). Weather conditions during the two-day period were relatively static. Total flux declines from 1.10 GW at midday to 0.99 GW in early evening (1800-1830MDT on Oct 11) to 0.92 GW later in the evening (2000-2030MDT on Oct 12). We tentatively attribute the systematic reduction in flux to radiational cooling associated with time of day. Our estimation of night background flux is less stable than the day time background estimates, perhaps reflecting accumulating water vapor in the boundary layer as temperatures cool. Based on two observations, the rate of change in background flux declines later in the evening.

Table N. Norris Geyser Basin Radiant Flux (2006)

BASINWIDE TOTALS	(Watts)	GW	
2006 TOTAL FLUX, DAY	1095870000.00	1.0959	
2006 GEOTHERMAL FLUX	113744094.58	0.1137	
2006 BACKGROUND FLUX	982125905.42	0.9821	
OCT 11, 1800-1830			% CHANGE
2006 TOTAL FLUX, NIGHT1	987961000	0.9880	-10.92%
2006 GEOTHERMAL FLUX	80803827.33	0.0808	-40.77%
2006 BACKGROUND FLUX	907157172.67	0.9072	-8.26%
OCT 12, 2000-2030			% CHANGE
2006 TOTAL FLUX, NIGHT2	919123443	0.9191	-19.23%
2006 GEOTHERMAL FLUX	43110262.70	0.0431	-163.84%
2006 BACKGROUND FLUX	876013180.30	0.8760	-12.11%

Table M. depicts remote sensing-based mean and standard deviation temperatures of several geothermal features from 2005. There are several noteworthy points to consider. First, hot features such as Gray Lakes, Frying Pan Spring, and Cistern show large apparent reductions in temperature at night, while cold targets such as Nuphar Lake do not. This is almost certainly due to steam. Consider Cinder Pool, which witnessed an apparent 43 degree change in night temperature between images obtained a few seconds apart. Second, variability in temperature is generally larger at night than day and larger for hot targets than cold, again probably due to steam. We suggest that colder ambient air temperatures and generally less wind at night result in significant, but highly variable effects on apparent temperatures of geothermal features. Similar factors are observed in 2006. Less clear is what occurs on the background sinter in the basin.

From chloride concentrations in rivers draining YNP (Ingebritsen et al. 2001), advective heat flux from the Yellowstone system is approximately 6.1GW; thermal areas northeast of the continental divide account for about 4.5GW. If advective heat flux from chloride and radiant heat flux from thermal imagery were equivalent, our results imply that approximately 5.5% of the heat flux for the area northeast of the continental divide comes from Norris Geyser Basin (4% on a Yellowstone system-wide basis). However, equivalency of the two flux estimates is not likely.

Table M. 2005 Mean Kinetic Temperatures- Norris

FEATURE	DAY/NIGHT	MDT	SCENE_ID	MEAN TEMP C	STDEV TEMP C
Grey lakes	day	1427	scen182	65.1	2.0
	day	1424	scen173	61.2	4.6
	nite	2220	scen619	28.0	1.3
	nite	2220	scen620	34.2	3.7
	day	1454	scen306	28.5	0.4
Semicentennial	day	1501	scen344	28.6	0.5
	nite	2255	scen748	29.1	0.8
	nite	2255	scen749	28.9	0.5
	day	1439	scen238	62.5	4.3
Frying Pan	day	1444	scen263	58.6	7.8
	nite	2238	scen685	57.0	8.5
	nite	2238	scen684	57.6	5.6
	day	1428	scen185	29.0	0.4
Reservoir	nite	2225	scen631	26.8	1.2
	nite	2233	scen666	19.2	0.2
	nite	2220	scen617	28.5	1.0
	day	1428	scen185	83.3	4.2
Cinder Pool	nite	2225	scen631	66.1	14.2
	nite	2233	scen666	23.2	2.0
Nuphar Lake	day	1416	scen137	8.8	0.3
	day	2434	scen172	9.4	0.2
	nite	2206	scen574	9.3	0.1
	nite	2210	scen585	9.4	0.1
Explosion Crater	day	1434	scen218	33.9	2.0
	day	1434	scen219	33.7	2.1
	nite	2233	scen666	24.4	2.5
	nite	2233	scen667	17.5	1.9
Cistern	day	1424	scen172	77.9	11.3
	day	1424	scen173	79.3	9.7
	nite	2210	scen584	32.6	15.3
	nite	2220	scen619	33.6	6.1

5.2. Defining Norris Geyser Basin and Depicting Sub-Basins

The geographic boundaries of Norris Geyser Basin have not been well-defined for the purposes of heat flux calculations. The Basin generally consists of open sinter, upland 'island's' with forest cover, and water. To define Norris Geyser Basin for the analysis described previously, we used the region-growing tool in ERDAS Imagine to 'grow' a

polygon from ‘seed’ pixels within the sinter background. The region growing tool evaluates the multi-spectral characteristics of pixels adjacent to the seed pixel by thresholding, and grows a polygon outward if adjacent pixels are similar to the seed pixel. It does this until no adjacent pixels are similar. Islands such as the timbered uplands can be included in the polygon if they become surrounded by selected pixels. We used the daytime 2005 imagery as the source for the region grow because 8-12cm of snow had fallen the night before and the geothermally-warmed sinter was the only snow-free area observed during field reconnaissance while the daytime imagery was acquired (picture below from morning of Oct 06, 3 hours prior to data acquisition). The result was a quasi-objective definition of Norris Geyser Basin that included the all of the connected snow-free area in the Basin plus the timbered islands surrounded by snow-free area.



Figure 4. October 06, 2005, 1000 local time.

For comparative purposes, the southwest corner of the Basin was truncated to match Hardy’s 2002 data (image below).

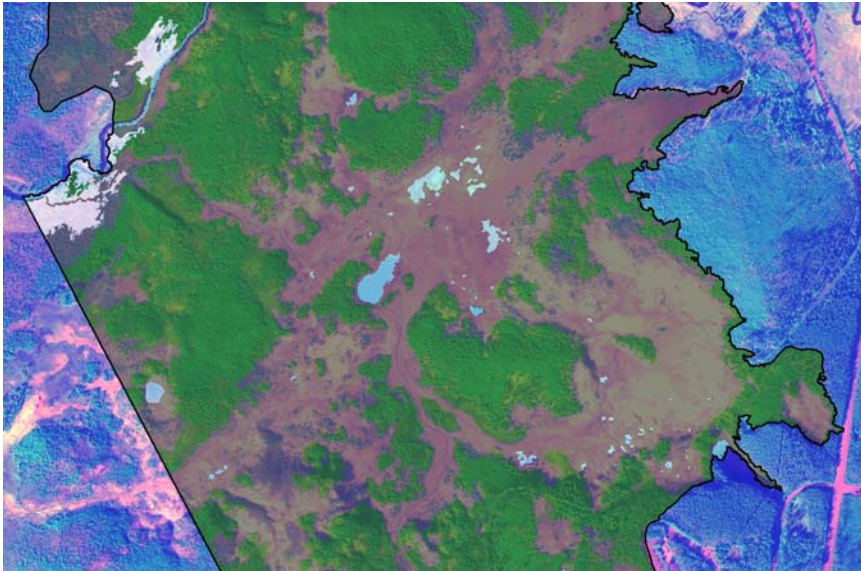


Figure 5. Core portion of Norris Geyser Basin as defined by region-grow methodology.

Sub-basins were also defined based on topographic breaks and with input from NPS staff. They are (shown below): Sulfur Dust, Lower Tantalus, The Reservoir-Upper Tantalus, 100 Springs Plain, Porcelain, Steamboat-Echinus-Emerald, Gray Lakes-Porkchop.

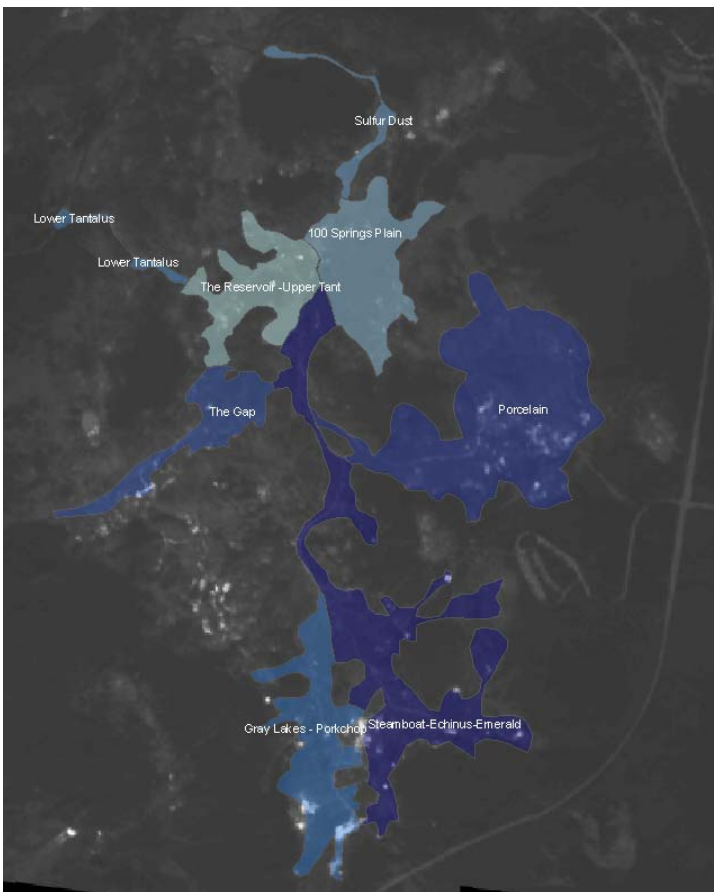


Figure 6. Sub-Basins of the Norris Geyser Basin.

6. Lessons Learned: Thermal Remote Sensing for Monitoring

Airborne thermal imaging provides a synoptic overview that cannot be obtained by other methods and it provides a permanent record of system state at time of acquisition. The spatial distribution of features is represented and some of the relative characteristics of features (such as temperature) are depicted. Within acquisition features are generally numerically comparable. However, there are a number of caveats to the latter statements that merit further discussion.

First, geothermal resources in Yellowstone come in two flavors: 1) discrete features with names and characteristic behaviors (generally involving water or steam); 2) large, diffuse bare ground areas (e.g., soil, sinter, calcite, etc...). As mentioned previously, the large, diffuse background appears more important to overall heat flux in Norris Geysir Basin than the discrete features due to their size. However, from an airborne remote sensing perspective, these two classes present different issues for monitoring. In general, the former class is plagued by mixed-pixel and n-size problems that are not consistent from frame-to-frame while attributes from the latter class of geothermal resources are confounded by well-known environmental variations (Short, 2009) as well as uncertainty regarding surface geothermics (Hochstein and Bromley, 2005).

6.1. “Discrete Geothermal Features”

Many of the geothermal water features are too small to provide robust thermal responses consistently (for example, Porkchop Geysir). Edge effects (mixed-pixel problem) obscure thermal properties of the feature and are variable from scene-to-scene. If steam is present there is a lower-likelihood of sampling a steam-free pixel (n-size problem).

With that said, for many of these features (Cinder, Emerald, Congress among them), their maximum DNs provide a reasonable representation of actual kinetic temperatures, as evidenced by the calibration curves with standard errors in the 5-9% of mean temperature range. Using the maximum DN also precludes the image analyst from having to reconcile GPS points of data loggers to the imagery, but also assumes temperature homogeneity within individual features. We observed only a few features (Thermal Explosion Crater, Green Dragon, Canary Spring) with large temperature gradients that are not explained by edge effects. These are generally bigger features perhaps with multiple heat sources.

Given the n-size and mixed-pixel problem, conventional image processing corrupts discrete thermal feature data both positionally and radiometrically. As example, the figure below shows Cinder pool before and after a standard nearest neighbor resample used during orthorectification.

CINDER POOL DIGITAL NUMBERS (2005)

932	910	906	907	925	941	948	968	997	930	932	906	907	925	941	968	997	1002
941	936	975	1072	1187	1154	1064	1022	1026	931	936	975	1072	1187	1154	1022	1026	1041
941	975	1289	1962	2604	2377	1521	1119	1063	920	975	1289	1962	2604	2377	1119	1063	1084
936	1176	2232	3487	4079	4036	2563	1265	1095	911	1176	2232	3487	4079	2563	1265	1095	1122
928	1418	2827	4083	4032	4035	3234	1383	1094	902	1312	2550	4046	4038	2790	1294	1094	1116
925	1312	2550	4046	4038	4089	2790	1294	1082	920	1041	1674	2466	2738	1771	1062	994	1054
920	1041	1674	2466	2738	2475	1771	1062	994	941	953	1065	1374	1475	1114	949	949	1052
941	953	1065	1374	1475	1329	1114	949	949	959	941	969	1038	1075	999	936	970	1039
959	941	969	1038	1121	1075	999	936	970	978	970	993	1023	986	927	883	922	964
975	962	971	1023	1037	986	927	883	922	973	983	1007	1003	896	857	829	856	858

Before Resample

After Resample

Consequently, manual extraction of DNs/Temps from individual geothermal features using calibrated “raw” imagery is the most reliable method of temperature extraction, but it is time-consuming and is not “repeatable” in the modern scientific sense unless minimum or maximum DNs are used. Measures of central tendency such as the arithmetic mean and median are less stable than min/maxs due to small sample sizes and the uncertainty regarding of steam and edge effects. In short, quality thematic data are obtainable manually for features of some minimum size (~80-100m² of surface area). Automated extraction of information content is difficult due to the resampling issues described previously and due to geolocation errors inherent to both acquisitions used in this study. Conventional image differencing for change detection is a non-starter with these data.

In sum, consistent radiometric estimates are possible for discrete geothermal features across multiple dates using two different instruments operating at different wavelengths. The standard error of the kinetic temperature estimates ranges from 2.3 - 4.1C (5-9% of mean temperature for the calibration targets (~40C)). With such information, one vision for monitoring features would be to define them in vector format and attribute their tables with temperature data from manual interpretation of “raw” imagery. This approach would be time consuming, particularly with frame-based images, perhaps necessitating the identification of a few key geothermal resources representative of larger systems that could be queried on a repetitive basis.

6.2. Vapor-Dominated Features

One objective of the 2006 mission was to acquire data from a vapor dominated system, e.g. Mud Volcano. Two sets of imagery were acquired, one day and one night. Three features from the Mud Volcano system were plumbed with thermal data loggers (Hot and Cold Sour Lake and Churning Cauldron). Each of the features was used in the DN – temperature calibration effectively (small residuals), implying that all were thermally similar to the water-dominated features used in the calibration. Based on a sample of 50 DNs, Churning Cauldron’s temperature was calculated at 71.8 ± 4.1 C (1 std deviation)

during day October 12, 2006. Temperature logger data for 4 days (Oct 11-14) revealed a very stable temperature source (69.96 ± 0.86 C). Inasmuch as Churning Cauldron is representative of vapor-dominated thermal features, it appears to behave thermally like features observed in the water-dominated system of Norris Geyser Basin. It is worth pointing out that Churning Cauldron is full of water, so it is not exactly like some of the vapor features described in other areas such as Hot Springs Basin.

6.3. "Geothermal Background Features"

As mentioned previously, geothermal background dominates total flux in Norris Geyser Basin. However, the quality of flux estimates for background is largely unknown and is susceptible to well-known variations in environmental conditions. Those variations are: [verbatim from N.M. Short's Remote Sensing Tutorial, 2009, http://rst.gsfc.nasa.gov/Sect9/Sect9_3.html]

"Interpreting thermal data and images of temperature distribution over an area is complex. In many instances, we must look for patterns of relative temperature differences rather than the absolute values, because of the many complex factors that make quantitative determinations difficult, such as:

- * Number and distribution of different material classes in an instantaneous field of view
- * Variations in the angle of thermal insolation relative to sensor position
- * ***Dependency of thermal response on composition, density and texture of the materials***
- * ***Emissivities of the surface materials***
- * Contributions from geothermal (internal) heat flux; usually small and local
- * Topographic irregularities including elevation, slope angle, and aspect (surface direction relative to the Sun's position)
- * ***Rainfall history, soil-moisture content, and evaporative cooling effects near the surface***
- * Vegetation canopy characteristics, including height, leaf geometry, and plant shape
- * Leaf temperatures as a function of evapotranspiration and plant stress
- * ***Near surface (1 to 3 meters) air temperature; relative humidity; and wind effects***
- * Temperature history of the atmosphere above the surface zone
- * Cloud-cover history (during heating/cooling cycle)
- * Absorption and re-emission of thermal radiation by aerosols, water vapor, and air gases"

We have highlighted a few of the factors above (in bold) that we believe require special attention in Norris Geyser Basin. Of particular note are moisture of the soil substrate, and boundary layer wind, humidity, and temperature. Hochstein and Bromley (2005) have demonstrated that total flux of steaming ground in a New Zealand geothermal field is produced by daily time-variable conductive heat flow (condensation in a thin surface layer (latent heat)) and convective heat flow (escaping water vapor). Convective heat flux can reach half of total flux and the partitioning of energy is largely dependent on soil moisture parameters between the boiling depth and the surface; notably a thin near-surface evaporation layer as well as enhanced condensation in the thin layer. IWe note

that total flux observed by Hochstein and Bromley (2005) ranged from 30 - 2000 watts/m² across a range of boiling temperature depths (4 meters to <0.1 meter). In Norris Geyser Basin, observed background radiant flux (with no adjustment for ‘background’) is in the 350-500 watts/m² range. If we assume an environmental background (no geothermal input) of about 200 watts/ m² then radiant geothermal flux is in the 150-300 watt/m² range. If these numbers represented about half of total flux (the other half being convective), boiling depth at Norris should be in the 1-2 meter range (presuming that Norris is similar to the Wairakei system in New Zealand, and that non-contact estimates of radiant flux track in situ conductive flux). We recognize that a lot of assumptions go into this logic but note the consistency between observations.

To move beyond back-of-napkin calculations, the thermal properties of hot ground in Norris Geyser Basin will require additional investigation in the context of non-contact thermal imaging. The behavior of soils with regard to thermal conductivity (under various moisture regimes) is not well understood in Norris Geyser Basin. More significantly, the relationship between geothermal conductive heat transfer at the surface and thermal imaging is largely unknown (e.g., we have no definition of ‘truth’ for geothermal ground). Even with ‘truth’ it may be difficult to perform quantitative change detection, given the between-acquisition differences in boundary layer moisture and temperature (and perhaps wind). These factors will always be difficult to control for even with additional research.

7. Observations and Recommendations:

7.1. General

- A clear definition of change is needed. Norris Geyser Basin is dynamic in ways that limit the utility of synoptic data for change detection, particularly in the context of acquisition environment changes.
- Having a pre-defined monitoring outline would help streamline image acquisition and processing alternatives.
- We are reasonably happy with temperature calculations for discrete features; in-situ data are important as ground truth. Diffuse background temperatures are more difficult to validate and we don’t have ground truth for these targets. Improvements could be made in emissivity, having a broader range of ground target temperatures, and pre-defined reporting units
- Pixel-based values (biophysical estimates) need to be used with caution. Errors in geolocation make neighborhood estimates or feature-based reporting more desirable. With that said, even subbasins might be too fine a neighborhood given geolocation errors along polygon edges.
- If specific features are of interest, consider future use of in-situ devices (cameras and radiometers) that do not require “mapping.”
- Processing is in the range of 2-times the cost of airborne data acquisition.
- The cost of acquisitions was ~\$30,000 each, with mobilizations from Redwood Falls, MN and Riverside, CA, respectively.

- Effectively all processing of '05 and '06 data followed the algorithm developed by Hardy with '02 data. Refinements were made particularly in de-striping, radiometric calibration (through application of more high-temperature ground targets), and rectification. Also note that the '05 data were collected using a different range setting on the TIR camera which reduced problems with pixel (dynamic range) saturation. However, the dynamic range of the 2005 acquisition resulted in saturation of targets >83C (440 total pixels).

7.2. Data Acquisition

- In situ calibration over the expected range of temperatures is critical.
- In situ flux data are needed for both geothermal and non-geothermal background.
- In situ flux measurements (oblique?) are worth pursuing.
- In field emissivity estimates of reference targets would be helpful.
- Hochstein and Bromley (2005) suggest that five plus consecutive dry days are ideal for stable geothermal flux measurements. This is a difficult window to hit in October with inherent aircraft logistical constraints.
- Try to acquire when T_a is not at dewpoint.
- It is not clear that night thermal imagery is superior to day imagery given moisture and geolocation issues.
- Generating “science” data takes months of processing; is the rate of improvement in data quality worth it to the user?
- Night-time imagery is difficult to rectify in the 3.5 micron bandpass; LWIR provides better background characterization at night, but doesn't make for better geolocation.
- Having optical bands is very helpful.
- No need to go smaller than ~3m pixel. E.g. don't assume that smaller pixels are going to fix n-size, mixed-pixel, and geolocation problems.

7.3. Image Processing

- Re-sampling is a real concern, especially if the processing stream requires multiple iterations of a resampling routine
- If destripe is needed, try to perform on raw data. Recommend against using ADS in the future due to sensor/amplifier issues.
- Calculate any radiometric values prior to rectification and mosaic; mosaics are potentially more useful as pictures than as data
- Scene sidelap and endlap are significant at increasing sample sizes for calibration (geometric and radiometric) but are troublesome when mosaicking scenes. A line scanner may prove more beneficial to monitoring than a frame-based system.
-

7.4. Thermal/Radiometric Calibration

- May be able to make calculations/calibrations from “raw” data best; but then have issues with the reporting unit (and “where”).

- Existing assumptions seem reasonable; difficult to improve on or ‘mitigate’; perhaps key is to work in a clear/dry atmosphere.
- Previously mentioned uncertainties regarding thermal characteristics of warm ground (e.g., emissivities, etc...).

7.5. Orthorectification

- Should be preceded by destripe/calibration/band-to-band registration, if needed (e.g., ADS data).
- Improvements can be made to improve geolocation accuracy; note the cost of processing and trade-offs of increases in accuracy near ground control point locations versus model instability at non-known locations.

7.6. Change Detection

- Define change.
- Mis-registration, resampling, mixed pixels, surface moisture, atmosphere are confounding variables
- Can we use thermocouple traces to determine change?
- Moisture content of substrate is a critical part of estimating emissivity; thus temperature and flux
- Overall, specific geothermal “features” are a small component of total heat flux from Norris Basin

7.7. Data Exploration

- Determine balance between “research” data and “picture” data
- If rapid turn-around is the key then ADS and similar vendors may be N/A— Fire Mapper was able to produce reasonable quick-look imagery for a fraction of their data. What is the value of that imagery?
- Trade-offs between geometric and radiometric fidelity are key.
- What is the feature being mapped or characterized; pixels are unreasonable as a resolution element given uncertainties in geolocation and radiometry.

8. References

Wicks, C.W., Thatcher, W. Dzurisin, D., and Svarc, J. 2005. Uplift, thermal unrest and magma intrusion at Yellowstone caldera. *Nature*, 440: 72-75.

Hardy, C. 2005. Characterizing thermal features from multi-spectral remote sensing data using dynamic calibration procedures. PhD Dissertation, University of Montana.

Ingebritsen, S.E., Galloway, D.L., Colvard, E.M., Sorey, M.L. and Mariner, R.H., Time-variation of hydrothermal discharge at selected sites in the western United States:

implications for monitoring, *Journal of Volcanology and Geothermal Research*, 111, 1-23, 2001.

Norton, D.R. and Friedman, I., Chloride flux and surface water discharge out of Yellowstone National Park, 1982-1989, U. S. Geological Survey Bulletin, Report: B 1959, 42 pp., 1991.

Riggan, P.J. and Hoffman, J.W. 2004. FireMapperTM: A Thermal-Imaging Radiometer for Wildfire Research and Operations. IEEE AC paper #1522, 12 pp.

Song, J. and Gao, W. 1999. An improved method to derive surface albedo from narrowband AVHRR satellite data: narrowband to broadband conversion. *Journal of Applied Meteorology*, 38: 239-249.